Improving the charge density normalization in Korringa–Kohn–Rostoker Green-function calculations

2008 J. Phys.: Condens. Matter 20 035220

(http://iopscience.iop.org/0953-8984/20/3/035220)

J. Phys.: Condens. Matter **20** (2008) 035220 (11pp) doi:10.1088/0953-8984/20/03/035220

Improving the charge density normalization in Korringa–Kohn–Rostoker Green-function calculations

Rudolf Zeller

Institut für Festkörperforschung, Forschungszentrum Jülich GmbH, D-52425 Jülich, Germany

E-mail: Ru.Zeller@fz-juelich.de

Received 21 September 2007, in final form 22 November 2007
Published 19 December 2007
Online at stacks.iop.org/JPhysCM/20/035220

Abstract

The truncation of angular momentum expansions in the Korringa–Kohn–Rostoker Green-function method introduces a charge normalization error and disallows calculation of the Fermi level and the charge density in a consistent manner. It is shown how this error can be compensated by Lloyd's formula, in particular if this formula is applied to normalize the Green function everywhere along the complex energy contour used for the integration of the charge density. The advantages of the improved normalization over the conventional one are illustrated by density-functional calculations for CrAs, the dilute magnetic semiconductor $Ga_{1-x}Mn_xN$ and a $Si_{12}Fe_8$ multilayer. It is shown that only the improved normalization leads to correct integer values of the magnetic moments in the half-metallic state of CrAs and $Ga_{1-x}Mn_xN$ and to a correct band alignment of Fe and Si states in the multilayer.

1. Introduction

The Korringa–Kohn–Rostoker (KKR) Green-function method requires truncations in angular momentum for the scattering t matrices and for the infinite sums, which appear in the multiple-scattering representation of the Green function. The angular momentum cut-off used for the t matrices is a well controlled numerical approximation, which usually rapidly converges with the number of angular momentum components taken into account. This cut-off simply means that the potential is approximated by a projection potential which is restricted to the lower angular momentum components of the wavefunctions. This approximation is not problematic since it goes along with other approximations for the potential, for instance the ones arising from numerical details and the choice of density-functional exchange–correlation potentials.

In contrast, the truncation of the Green-function representation presents a real problem. Because higher angular momentum contributions to the charge density are not included, the charge density is not normalized correctly. In metals the small missing or extra charge can be counterbalanced by an adjustment of the Fermi level and the required shift of the Fermi level is usually small and often negligible. In insulators and semiconductors, however, the charge does not change if the Fermi level is varied inside the band gap and the adjustment inevitably puts the Fermi level either into the valence or conduction band. The incorrect position of the Fermi level can lead to systematically incorrect physical properties because it makes the systems metallic and their semiconducting or insulating behaviour is lost.

The problem has been recognized in the past [1–7] and Lloyd's formula has been suggested as a remedy. Lloyd's formula can be used to determine the Fermi level since it directly gives the integrated density of states. By implicit summation over all angular momenta Lloyd's formula avoids the error which is caused by the truncation of the infinite sums in the multiple-scattering representation of the Green function. However, one difficulty remains if Lloyd's formula is used to determine the Fermi level. Lloyd's formula cannot be used for the charge density but only for the total charge integrated over all space. If the Fermi level determined by Lloyd's formula is used together with the charge density calculated in the usual way from the truncated angular momentum expansion of the Green function, then this charge density is not normalized correctly and charge neutrality is prevented. Therefore, the charge density must be modified and several modifications have been suggested. In muffin-tin calculations the missing or extra charge can be hidden in the interstitial region, but in atomic sphere or full potential calculations this option is not available. Here the missing or extra charge can be put into

the highest angular momentum component or can be added as a constant average in all space. Another possibility is the multiplication of the charge density by a constant factor. A common disadvantage of these modifications is that they do not distinguish between states which are mainly responsible for the charge density normalization error and states with small contributions to the error. For instance, if the main error arises from the semi-core states of one atom in the crystal, it is desirable that only these states are renormalized, but not all states of all atoms.

The purpose of this paper is to present a more satisfactory modification for the charge density. The idea is to apply a normalization in a similar way as is done in electronic structure calculations with basis-set methods. In basis-set methods a finite subset of basis functions is chosen from an infinite complete set and used for the expansion of the wavefunctions (eigenfunctions). For different subsets the wavefunctions contain different partial contributions from the individual basis functions, but the overall normalization of the wavefunctions is always kept at the correct value and the charge density calculated by a sum over wavefunction contributions is always normalized correctly. A basically similar procedure is used in the traditional, wavefunction-based KKR method, where the infinite-dimensional KKR matrix is truncated to the subspace of low angular momenta and the wavefunctions are normalized in this subspace [8]. This procedure transfers the weight of neglected higher angular momenta to the lower ones taken into account and leads to a correct normalization of the charge density.

The KKR Green-function method avoids wavefunctions for the calculation of the charge density, which is obtained alternatively by energy integration over the Green function, usually in the complex energy plane. The use of the Green function instead of wavefunctions provides an economic and practical way to treat solids with reduced symmetry, for example impurities in otherwise ordered host crystals, surfaces or layered systems, since the Green function of a system is related to the Green function of simpler reference system by an algebraic Dyson equation. On the other hand, the use of the Green function introduces the charge normalization error discussed above. Recently it was proposed [7] that the normalization error could be compensated if the values of the KKR Green function at each integration mesh point along the complex energy contour are multiplied with appropriate factors and that these factors could be determined by the energy derivative of Lloyd's formula. However, it was not clear how the divergence arising from the real part of the Green function along the contour could be treated in a satisfactory manner.

The aim of the present work was to find a way to deal with the divergence of the real part and to investigate how the calculated results are affected if normalization factors determined by the derivative of Lloyd's formula are used to normalize the KKR Green function. After giving the basic equations in section 2, the treatment of the divergence is explained in detail in section 3. Section 4 contains the numerical details and section 5 is used to illustrate the advantage of the proposed normalization for the calculated spin moments and densities of states of the ferromagnetic half-metal CrAs, the dilute magnetic semiconductor $Ga_{1-x}Mn_xN$ and a $Si_{12}Fe_8$ multilayer. The main result is that the proposed normalization leads to correct integer values for the moments in the half-metallic states of CrAs and $Ga_{1-x}Mn_xN$ and to a correct band alignment of Fe and Si states in the multilayer.

2. Basic equations

The KKR Green-function method determines the charge density ρ around a given atomic position $\mathbf{R}^n$ from the imaginary part of the Green function G by energy integration as

$$\rho(\mathbf{r}+\mathbf{R}^n) = -\frac{2}{\pi}\mathrm{Im}\int_{-\infty}^{E_\mathrm{F}} \mathrm{d}E\, G(\mathbf{r}+\mathbf{R}^n, \mathbf{r}+\mathbf{R}^n; E) \quad (1)$$

or, to take advantage of temperature broadening, as

$$\rho(\mathbf{r}+\mathbf{R}^n) = -\frac{2}{\pi}\mathrm{Im}\int_{-\infty}^{\infty} \mathrm{d}E\, f(E, E_\mathrm{F}, T) G(\mathbf{r}+\mathbf{R}^n, \mathbf{r}+\mathbf{R}^n; E), \quad (2)$$

where $\mathbf{r}$ denotes cell-centred coordinates and $f(E, E_\mathrm{F}, T) = (1+\exp(\beta(E-E_\mathrm{F})))^{-1}$ the Fermi–Dirac function for inverse temperature $\beta = (kT)^{-1}$ and Fermi level E_F. Atomic units are used throughout this paper and the factor 2 arises from spin degeneracy, which is assumed to simplify the following equations. The extension to spin-polarized calculations is straightforward. A powerful technique to calculate (1) and (2) is contour integration in the complex energy plane [9, 10]. Away from the real energy axis the integrands are smooth functions of energy because of the analytical behaviour of the Green function. Therefore, the use of complex energies considerably reduces the numerical effort, in particular for periodic systems, where many fewer $\mathbf{k}$ points are required for Brillouin-zone integrations. Numerically the integrals in (1) and (2) can be evaluated by integration rules of the form

$$\rho(\mathbf{r}+\mathbf{R}^n) = -\frac{2}{\pi}\sum_i \mathrm{Im}[w_i G(\mathbf{r}+\mathbf{R}^n, \mathbf{r}+\mathbf{R}^n; E_i)] \quad (3)$$

with suitably chosen complex valued integration points E_i and weights w_i, which depend on the Fermi level E_F. For $T \neq 0$ the integration points conveniently include some of the Matsubara energies $E_n = E_\mathrm{F} + (2n-1)\mathrm{i}\pi kT, n = 1, 2, \ldots$. The Green function for equal space arguments can be expressed as

$$G(\mathbf{r}+\mathbf{R}^n, \mathbf{r}+\mathbf{R}^n; E) = \sum_L^\infty R_L^n(\mathbf{r}; E) S_L^n(\mathbf{r}; E) + \sum_{LL'}^\infty R_L^n(\mathbf{r}; E) G_{LL'}^{nn}(E) R_{L'}^n(\mathbf{r}; E), \quad (4)$$

where the notation of [7, 11] is used with the usual abbreviation L for the pair l and m of angular momentum indices. $R_L^n(\mathbf{r}; E)$ and $S_L^n(\mathbf{r}; E)$ denote regular and irregular single-scattering solutions and $G_{LL'}^{nn'}(E)$ Green-function matrix elements, which can be obtained from the matrix elements $G_{LL'}^{r,nn'}(E)$ of a suitably chosen reference system by an algebraic Dyson equation. The position of the Fermi level E_F is determined by the condition that the total charge

$$Q = \sum_n \int_n \mathrm{d}\mathbf{r}\, \rho(\mathbf{r}+\mathbf{R}^n) \quad (5)$$

has the required value. For instance, in charge neutral systems the electronic charge Q must cancel the sum of nuclear charges. The problem in standard KKR Green-function calculations arises because the multiple-scattering expression (4) is truncated as

$$\tilde{G}(\mathbf{r}+\mathbf{R}^n,\mathbf{r}+\mathbf{R}^n;E)=\sum_{L}^{l_{\max}}R^n_L(\mathbf{r};E)S^n_L(\mathbf{r};E)+\sum_{LL'}^{l_{\max}}R^n_L(\mathbf{r};E)G^{nn}_{LL'}(E)R^n_{L'}(\mathbf{r};E) \quad (6)$$

with a finite angular momentum cut-off $l_{\max}$ and because the charge density is then approximated by

$$\tilde{\rho}(\mathbf{r}+\mathbf{R}^n)=-\frac{2}{\pi}\sum_i \mathrm{Im}[\tilde{w}_i\tilde{G}(\mathbf{r}+\mathbf{R}^n,\mathbf{r}+\mathbf{R}^n;\tilde{E}_i)]. \quad (7)$$

Here the integration points $\tilde{E}_i$ and weights $\tilde{w}_i$ differ from E_i and w_i, since they depend on a changed Fermi level $\tilde{E}_\mathrm{F}$ determined by the condition that total charge

$$\tilde{Q}=\sum_n\int_n \mathrm{d}\mathbf{r}\,\tilde{\rho}(\mathbf{r}+\mathbf{R}^n) \quad (8)$$

agrees with the required value Q. In insulators and semiconductors this condition can be satisfied only if the Fermi level $\tilde{E}_\mathrm{F}$ is shifted into the valence or conduction band with the unpleasant consequence that these systems are treated as metals. Varying $\tilde{E}_\mathrm{F}$ inside the band gap has a negligible effect on $\tilde{Q}$ and cannot be used to satisfy the condition $\tilde{Q}=Q$.

The error for the total charge arising from the truncation in (6) is avoided if the total charge is calculated by the use of Lloyd's formula

$$N(E)=N^r(E)+\frac{2}{\pi}\sum_n \ln\det|\Delta\alpha^n_{LL'}(E)|-\frac{2}{\pi}\ln\det|\delta^{nn'}_{LL'}-G^{r,nn'}_{LL'}(E)\Delta t^{n'}_{LL'}(E)|, \quad (9)$$

here given in the notation of [7, 12], according to the expression

$$Q=\mathrm{Im}\int_{-\infty}^{\infty}\mathrm{d}E\,f(E,E_\mathrm{F},T)n(E)=\sum_i \mathrm{Im}[w_i n(E_i)]. \quad (10)$$

Here $n(E)$ denotes the energy derivative of $N(E)$ and can be understood as a generalization of the density of states into the complex plane since Im $n(E)$ agrees with the density of states for real energies. In (9) the quantities $N^r(E)$ and $G^{r,nn'}_{LL'}(E)$ are the 'integrated density of states' and the Green-function matrix elements of a reference system. The changes $\Delta t^n_{LL'}(E)$ and $\Delta\alpha^n_{LL'}(E)$ of the t and α matrices at site n are defined with respect to the reference system by integrals over products of regular or irregular single-scattering solutions as described in detail in the appendix.

It is clear that (9) cannot be evaluated without angular momentum truncation of the Δt and $\Delta\alpha$ matrices. However, contrary to the $l_{\max}$ truncation in (6), the neglect of matrix elements with $l > l_{\max}$ in Δt and $\Delta\alpha$ causes no difficulty, since it simply means a replacement of the potential by a projection potential acting in the subspace $l \leqslant l_{\max}$. In this sense formula (9), which can be evaluated with matrices of finite dimension in angular momentum, delivers exact results so that for the projection potential Lloyd's formula always gives the correct charge Q with its integer value if E_F is varied inside the band gap.

Note that for periodic crystals with an infinite number of atoms (9) cannot be used directly because it gives an infinite result. Then $N(E)$ defined per unit cell as

$$N(E)=N^r(E)+\frac{2}{\pi}\sum_\nu \ln\det|\Delta\alpha^\nu_{LL'}(E)|-\frac{2}{\pi V_\mathrm{BZ}}\int_\mathrm{BZ}\mathrm{d}\mathbf{k}\ln\det|\delta^{\nu\nu'}_{LL'}-G^{r,\nu\nu'}_{LL'}(\mathbf{k};E)\Delta t^{\nu'}_{LL'}(E)| \quad (11)$$

is used, where the integral is over the Brillouin zone and the site indices ν, ν' are restricted to the basis sites in the unit cell.

It is now an important question how the Fermi level determined by Lloyd's formula can be made consistent with the charge density. The difficulty is that Lloyd's formula can be used only for the space integrated total charge but not for the space resolved charge density. Thus the truncation in (6) can only be avoided for the determination of E_F, but not for the calculation of the charge density. If the correct Fermi level E_F and the resulting mesh points E_i and weights w_i are used together with the truncated Green function (6), the charge density (3) is not normalized correctly. The central idea of this paper is the introduction of normalization factors λ_i along the integration contour and the calculation of the charge density as

$$\rho_\lambda(\mathbf{r}+\mathbf{R}^n)=-\frac{2}{\pi}\sum_i\lambda_i\,\mathrm{Im}[w_i\tilde{G}(\mathbf{r}+\mathbf{R}^n,\mathbf{r}+\mathbf{R}^n;E_i)] \quad (12)$$

with integration points E_i and weights w_i consistent with the Fermi level determined by Lloyd's formula. The factors λ_i are determined by the condition

$$-\frac{2}{\pi}\lambda_i\sum_n\int_n\mathrm{d}\mathbf{r}\,\mathrm{Im}[w_i\tilde{G}(\mathbf{r}+\mathbf{R}^n,\mathbf{r}+\mathbf{R}^n;E_i)]=\mathrm{Im}[w_i n(E_i)], \quad (13)$$

where $n(E)$ is the exact energy derivative of $N(E)$ given by (9) or (11). If both sides of (13) are summed over i, the use of (12) and (10) leads to

$$\sum_n\int_n\mathrm{d}\mathbf{r}\,\rho_\lambda(\mathbf{r}+\mathbf{R}^n)=Q, \quad (14)$$

which shows that the charge density ρ_λ gives the correct charge and thus is consistent with the Fermi level determined by Lloyd's formula.

3. Treatment of divergent terms

Unfortunately, the simple idea expressed by (12) and (13) cannot be applied straightforwardly in complex contour integrations. For complex contours the weights w_i are complex quantities and thus both real and imaginary parts of $\tilde{G}$ contribute. Here it is important to realize that the real part of (6) diverges for $l_{\max}\to\infty$. The divergence arises from the first

sum and is a consequence of the source term in the differential equation $[-\nabla^2_{\mathbf{r}} + V(\mathbf{r}) - E]G(\mathbf{r}, \mathbf{r}'; E) = -\delta(\mathbf{r} - \mathbf{r}')$ for the Green function. Since the real part of $\tilde{G}$ increases towards infinity with increasing $l_{\max}$, the factors λ_i determined by use of (13) vanish in the limit $l_{\max} \to \infty$. It is clear that such a limiting behaviour is not the desired result, since useful normalization factors are expected to satisfy $\lambda_i = 1$ in the limit $l_{\max} \to \infty$ so that they become less and less important with increasing $l_{\max}$. To obtain such factors, the contribution of a suitably chosen reference system can be subtracted from both sides of (13), since by subtraction the divergence is cancelled. The easiest reference system is potential free space with the Green function G^0 which is given in all cells n for equal space arguments by

$$G^0(\mathbf{r} + \mathbf{R}^n, \mathbf{r} + \mathbf{R}^n; E) = \sum_L^{\infty} J_L(\mathbf{r}; E) H_L(\mathbf{r}; E). \tag{15}$$

Here $J_L(\mathbf{r}; E) = j_l(r\sqrt{E})Y_L(\mathbf{r})$ and $H_L(\mathbf{r}; E) = -\mathrm{i}\sqrt{E}h_l^{(1)}(r\sqrt{E})Y_L(\mathbf{r})$ are the 'single-scattering' solutions in free space which are defined as products of spherical harmonics Y_L with spherical Bessel functions j_l and Hankel functions $h_l^{(1)}$. Contrary to (4) no double sum appears in (15) because the on-site Green-function matrix elements $G^{0,nn}_{LL'}(E)$ vanish for potential free space. An equation for free space, which can be subtracted from (13) to achieve a cancellation of the divergence, is given by

$$\begin{aligned} &-\frac{2}{\pi}\sum_n \int_n \mathrm{d}\mathbf{r}\, \mathrm{Im}[w_i \tilde{G}^0(\mathbf{r} + \mathbf{R}^n, \mathbf{r} + \mathbf{R}^n; E_i)] \\ &= \mathrm{Im}[w_i n^0(E_i)] - \mathrm{Im}[w_i \Delta n^0(E_i)]. \end{aligned} \tag{16}$$

Here $\tilde{G}^0$ is defined by truncating the sum in (15) to terms in the subspace $l \leqslant l_{\max}$ and $n^0(E)$ denotes the energy derivative of the 'integrated density of states' $N^0(E)$ for free space. Contrary to (13) the last equation does not contain normalization factors. The effect of the truncation is explicitly taken into account by the last term

$$\begin{aligned} &\mathrm{Im}[w_i \Delta n^0(E_i)] \\ &= -\frac{2}{\pi}\sum_n \int_n \mathrm{d}\mathbf{r}\, \mathrm{Im}\left[w_i \sum_{l>l_{\max}}^{\infty} J_L(\mathbf{r}; E_i) H_L(\mathbf{r}; E_i)\right]. \end{aligned} \tag{17}$$

It would be helpful to avoid the infinite sum in this equation. However, as discussed in the appendix, this does not seem to be possible. Fortunately, the contribution of (17) to the total charge is rather small, for instance if $l_{\max} = 3$ is used it is smaller than 0.0006 electrons per atom for the materials studied below. Thus the procedure proposed here for improving the charge density normalization consists of two steps. In the first step (17), which includes the higher angular momentum contributions of the free space Green function, is neglected and preliminary factors $\lambda_i^\star$ are determined by

$$\begin{aligned} &-\frac{2}{\pi}\lambda_i^\star \sum_n \int_n \mathrm{d}\mathbf{r}\, \mathrm{Im}[w_i \tilde{G}(\mathbf{r} + \mathbf{R}^n, \mathbf{r} + \mathbf{R}^n; E_i)] \\ &= \mathrm{Im}[w_i n(E_i)] - \mathrm{Im}[w_i n^0(E_i)] \\ &\quad + \frac{2}{\pi}\sum_n \int_n \mathrm{d}\mathbf{r}\, \mathrm{Im}[w_i \tilde{G}^0(\mathbf{r} + \mathbf{R}^n, \mathbf{r} + \mathbf{R}^n; E_i)], \end{aligned} \tag{18}$$

where the difference of $n(E_i)$ and $n^0(E_i)$ is directly given by the energy derivative of Lloyd's formula (9). In the second step the preliminary factors are scaled as

$$\lambda_i = \lambda_i^\star Q/Q^\star, \tag{19}$$

where Q is the charge calculated by Lloyd's formula and $Q^\star$ the charge calculated according to (12), but with factors $\lambda_i^\star$ instead of λ_i. This procedure seems to be well justified since the relative change between Q and $Q^\star$ was always smaller than 0.01% in the calculations for the materials studied below.

4. Numerical details

The calculations were carried out with the spin-polarized relativistic tight-binding (TB) KKR package [13] in a modified version adapted for the evaluation of Lloyd's formula and for the normalization procedure explained above. The program, which is based on the screened KKR formalism [14–16] as described in [17, 18], uses a partitioning of space into Voronoi cells around atomic positions and an expansion of potential and charge density into spherical harmonics up to $2l_{\max}$. Charge density integrals over cells were done as described in the appendix by the use of shape functions [19], which are expanded into spherical harmonics [20, 21]. To improve the convergence of the spherical harmonic expansions, the zincblende geometry of the studied systems was described by face-centred-cubic unit cells with two occupied and two empty basis sites along the (111) direction. In this way the geometric arrangement of all sites represents a body-centred-cubic lattice and the Voronoi cells agree with usual Wigner–Seitz cells of this lattice. The screened (TB) structure constants $G^{r,\nu\nu'}_{LL'}(\mathbf{k}, E)$ were determined in real space by clusters consisting of 169 repulsive muffin-tin potentials with height 8 Ryd in the appropriate body-centred-cubic arrangement. The single-scattering solutions R^n_L and S^n_L were calculated by first solving the radial Schrödinger equation for the spherical part of the potential and then iterating a Born series (up to fourth order) to include the non-spherical part as described in [18, 22].

The calculations were done for a non-zero electronic temperature $T = 400$ K with a complex energy integration contour (for details see the appendix) and the mesh points on the contour were chosen to be dense enough that total energies and magnetic moments were calculated with errors per atom smaller than 0.01 mRyd and 0.0001 μ_B. For this accuracy a total of 40 mesh points was enough for CrAs and the $Si_{12}Fe_8$ multilayer, whereas 48 mesh points were necessary for $Ga_{1-x}Mn_xN$ due to the 3d states of Ga, which were treated as valence states inside the integration contour. The 3d states of As, the 3s and 3p states of Cr, Mn, Fe, Ga and As, the 2s and 2p states of Si and the 1s states of N, as well as all deeper lying states were treated in an atomic fashion using the spherical part of the potential confined to non-overlapping spheres. All higher lying states, in particular the 3d states of Ga, the 4s states of As and the 2s states of N, were included in the contour.

The energy derivative of Lloyd's formula was calculated by exploiting the Riemann–Cauchy conditions for analytical

functions, which state that any analytical function $f(z) = u(z) + \mathrm{i}v(z)$ of the complex variable $z = x + \mathrm{i}y$ with real $u(z)$ and $v(z)$ must satisfy the equations $\frac{\mathrm{d}u}{\mathrm{d}x} = \frac{\mathrm{d}v}{\mathrm{d}y}$ and $\frac{\mathrm{d}u}{\mathrm{d}y} = -\frac{\mathrm{d}v}{\mathrm{d}x}$. This means that the derivative of (9) and (11) can be obtained as

$$\frac{\mathrm{d}N(E)}{\mathrm{d}E} = \frac{\mathrm{dRe}N(E)}{\mathrm{dRe}E} - \mathrm{i}\frac{\mathrm{dRe}N(E)}{\mathrm{d\,Im}E} \tag{20}$$

by derivatives of the single-valued real part of $N(E)$ in the directions parallel and perpendicular to the real axis. In this manner the multivalued imaginary part of the complex logarithm with the usually difficult determination of its correct branch was avoided [7]. The derivatives in (20) were evaluated by numerical differentiation with a symmetric two-point formula

$$\frac{\mathrm{d}N(E)}{\mathrm{d}E} = \frac{1}{2h}[N(E+h) - N(E-h)] \tag{21}$$

with the step size chosen as $h = \pi kT/100$, which leads to accurate results as shown in [7].

For the Brillouin-zone integration a uniformly distributed **k**-point mesh was used and the number of **k** points was chosen so that calculated total energies and magnetic moments were converged within 0.01 mRyd and 0.0001 μ_B per atom. It has been observed [7, 23] that Lloyd's formula requires a dense **k**-point mesh for the slowly converging Brillouin-zone integration. Since free space has partially occupied bands at all positive energies, the slow convergence for $N(E) - N^0(E)$ in (11) occurs not only for energies in valence and conduction bands but also in gaps as a consequence of the metallic like behaviour of $N^0(E)$. Here a repulsive reference system, which has no eigenstates in the relevant energy range, can improve the convergence of the Brillouin-zone integration considerably [7]. In the present work a repulsive system consisting of muffin-tin potentials of height 8 Ryd was used to calculate $N(E) - N^0(E)$ by the difference of $N(E) - N^r(E)$ and $N^r(E) - N^0(E)$. Here $N(E) - N^r(E)$ converges sufficiently well and $N^r(E) - N^0(E)$ can be calculated using many **k** points since the repulsive system is equivalent to a body-centred cubic structure with only one atom per unit cell.

Density-functional theory was used for all calculations with the local-density approximation (LDA) in the form given by Vosko *et al* [24]. Since the charge density normalization explained above is applicable for any choice of the exchange–correlation potential, the LDA was preferred to avoid the usually cumbersome numerical treatment of more sophisticated exchange–correlation potentials. To simplify the calculations further, all relativistic effects were also neglected.

5. Results and discussion

The advantages of the improved charge density normalization are now illustrated for some model systems, for the transition-metal pnictide compound CrAs, which becomes a half-metallic ferromagnet if it is grown in the zincblende structure epitaxially on GaAs(100) substrates [25], for the semiconductor GaN doped with Mn impurities and for a multilayer system consisting of Si and Fe layers. CrAs was chosen to illustrate that the proposed normalization leads to integer moments, which directly reveal the half-metallic state at expanded volume, whereas in previous KKR Green-function calculations [26, 27] additional band structure calculations or density-of-states inspections were necessary to find half-metallic states. Mn-doped GaN was chosen to show that the proposed normalization prevents large errors of the magnetic moment, which arise if charge neutrality is obtained by an adjusted Fermi level. These error are particularly large for small Mn concentration since the incorrect normalization of all host states must be compensated by a dilute number of available impurities. Finally, the SiFe multilayer was chosen to illustrate that in semiconductor–metal junctions a correct alignment of the electronic states in the semiconducting and metallic regions is obtained if normalization factors λ_i determined by (18) and (19) are used, whereas an adjustment of the Fermi level leads to an even qualitatively incorrect band alignment.

Table 1. Calculated moments for CrAs at different lattice parameters. The moments $\tilde{M}$, M_λ and $M_{\overline{\lambda}}$ are obtained from the charge densities $\tilde{\rho}$, ρ_λ and $\rho_{\overline{\lambda}}$ defined in the text.

a (nm)	$\tilde{M}$ (μ_B)	M_λ (μ_B)	$M_{\overline{\lambda}}$ (μ_B)
0.5338	2.3031	2.2889	2.2862
0.5393	2.3814	2.3788	2.3748
0.5448	2.5030	2.5091	2.5042
0.5503	2.6583	2.6641	2.6588
0.5558	2.8321	2.8346	2.8297
0.5614	2.9371	2.9670	2.9652
0.5669	2.9505	2.9981	2.9980
0.5724	2.9502	2.9999	2.9999
0.5779	2.9493	3.0000	3.0000
0.5834	2.9485	3.0000	3.0000

For comparison the results presented below were calculated by using three different charge densities $\tilde{\rho}$, ρ_λ and $\rho_{\overline{\lambda}}$, which differ by the method applied to obtain charge neutrality. Here $\tilde{\rho}$ denotes the charge density calculated with a simple Fermi level shift, while ρ_λ and $\rho_{\overline{\lambda}}$ denote charge densities calculated with normalization of the Green function along the complex energy integration contour. For ρ_λ the normalization factors were obtained by (18) and (19), whereas for $\rho_{\overline{\lambda}}$ a mesh point independent 'average' factor $\overline{\lambda} = Q/\tilde{Q}$ was used, which means that the charge density obtained from the truncated Green function is simply multiplied by $\overline{\lambda}$. Here Q is the charge calculated by Lloyd's formula and $\tilde{Q}$ the charge calculated by (7) and (8), but with mesh points E_i and weights w_i, which are appropriate for the correct Fermi level. Note that for the present spin-polarized calculation the normalization factors are determined for the spin-resolved Green function, which makes them different for the two spin directions.

5.1. CrAs

The calculated magnetic moments per zincblende unit cell are shown in table 1. The moments increase up to a lattice parameter $a = 0.5669$ nm and are approximately constant at larger lattice parameters. Here the expected integer value of 3.00 μ_B, characteristic for a half-metallic ferromagnet, is obtained if Lloyd's formula is used, whereas the moments

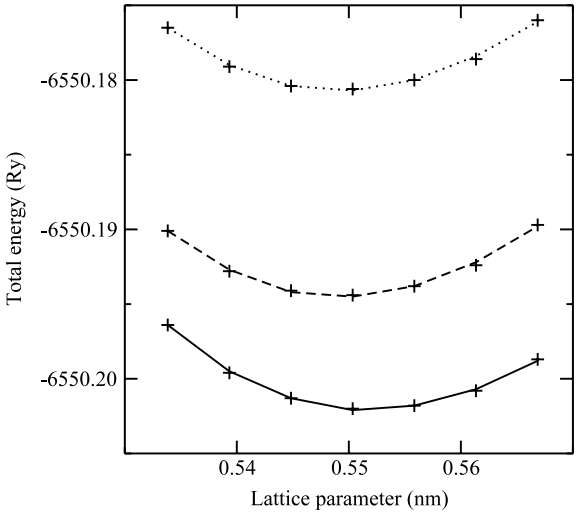

Figure 1. Calculated total energy for CrAs as a function of the lattice parameter. The dashed, solid and dotted lines are for the charge densities $\tilde{\rho}$, ρ_λ and $\rho_{\overline{\lambda}}$ defined in the text and were obtained by fits to a Birch–Murnaghan equation of state. The crosses indicate the calculated results.

saturate at a non-integer value of about 2.95 μ_B if the Fermi level is adjusted. The equally good performance of the charge densities ρ_λ and $\rho_{\overline{\lambda}}$ is not surprising, since integer moments are a direct consequence of an integer number of minority states. This integer number is guaranteed by Lloyd's formula alone, if the Fermi level is in a gap of these states, and is not changed if different normalization methods are chosen to make the charge density consistent with the Fermi level. Table 1 shows that the transition to a half-metallic state occurs just above $a = 0.5669$ nm. This is somewhat larger than in other recent density-functional calculations (see, for instance, Sasioglu *et al* [28] and references cited therein) which, however, use different approximations like spherical potentials, scalar relativistic solutions of the Schrödinger equation or generalized gradient approximations for exchange and correlation and thus cannot be compared directly with the present calculations.

The effect of the different charge densities $\tilde{\rho}$, ρ_λ and $\rho_{\overline{\lambda}}$ on the calculated equilibrium properties of CrAs was investigated by total energy calculations. For this purpose the total energy was calculated for seven lattice parameters in the vicinity of the estimated equilibrium lattice parameter $a = 0.550$ nm. To reduce inaccuracies arising from changes of the atomically treated core states [29], these states were always confined to muffin-tin spheres with the same radius 2.18 a_B. The results, which are shown in figure 1 by crosses, were fitted to a Birch–Murnaghan equation of state [30]

$$E_{\mathrm{tot}} = \sum_{m=1}^{4} c_m a^{2-m} \tag{22}$$

with four parameters c_m determined by least square minimization. Table 2 shows the total energy minimum, the equilibrium lattice parameter and the bulk modulus at the equilibrium lattice parameter obtained from the fitted equation of state. The calculated lattice parameters agree to within 0.5% and the bulk moduli, which are usually more sensitive to numerical approximations, to within 5%. The agreement indicates that for the calculation of equilibrium lattice parameters and bulk moduli it is relatively unimportant how charge neutrality is obtained. This insensitivity is probably a general trend and explains why previous KKR Green-function results for semiconductors [31], which were calculated without using Lloyd's formula, were found to be in accurate agreement with the results of full potential linear augmented plane-wave (FLAPW) calculations.

Table 2. Calculated equilibrium lattice parameters a, bulk moduli B and minima E_{min} of the total energy of CrAs for the charge densities $\tilde{\rho}$, ρ_λ and $\rho_{\overline{\lambda}}$ defined in the text.

Density	a (nm)	B (GPa)	E_{min} (Ryd)
$\tilde{\rho}$	0.5495	59.3	−6550.194 504
ρ_λ	0.5519	56.3	−6550.202 115
$\rho_{\overline{\lambda}}$	0.5493	57.5	−6550.180 716

5.2. $Ga_{1-x}Mn_xN$

The dilute magnetic semiconductor $Ga_{1-x}Mn_xN$ was treated in supercell geometry. The zincblende structure with lattice parameter $a = 0.452$ nm was preferred to the more complicated wurtzite structure since rather similar charge density normalization effects are expected in both structures. Two supercell sizes with 16 and 32 atoms corresponding to Mn concentrations of $x = 1/8$ and $1/16$ were investigated. The supercell with 32 atoms was chosen identical to the one used by de Paiva *et al* [32] (displayed in figure 1 of their paper). The supercell with 16 atoms was chosen to be half as wide in the x direction. Local relaxations caused by the Mn atoms were not considered, since according to [33] they have a negligible effect on the electronic and magnetic properties and they are not important for the present illustrative purpose.

In dilute magnetic semiconductors the states available at the Fermi level arise from the magnetic impurities inserted into the semiconductors. If charge neutrality is enforced by a Fermi level shift, the occupancy of the impurity states changes, whereas almost no change occurs in the occupancy of the semiconducting states. In Mn-doped GaN only minority spin states are available at E_F and by a Fermi level shift the magnetic moment changes. The change can be very large if the amount of Mn impurities is very small. For instance, if the Green function is truncated at $l_{\mathrm{max}} = 3$, the number-of-states error [7] per GaN unit cell is 0.052. This leads to a reduction of the number of occupied Mn majority states by about $0.052/x$ if charge neutrality is obtained by a Fermi level shift. The estimated total magnetic moment per unit cell is then about 3.6 μ_B for $x = 1/8$ and 3.2 μ_B for $x = 1/16$. These estimates agree rather well with the calculated results shown in table 3 for the charge density $\tilde{\rho}$. Thus the use of a Fermi level adjustment to obtain charge neutrality leads to unacceptably large errors of the magnetic moment.

The unphysical reduction of the magnetic moment is avoided if the Fermi level is determined by Lloyd's formula and if normalization factors for the KKR Green function are

Table 3. Local magnetic moments M_{loc} inside the Mn cell and total magnetic moments M_{tot} in $Ga_{1-x}Mn_xN$ supercells calculated for the charge densities $\tilde{\rho}$, ρ_λ and $\rho_{\overline{\lambda}}$ defined in the text.

	$x = 1/8$		$x = 1/16$	
Density	M_{loc} (μ_B)	M_{tot} (μ_B)	M_{loc} (μ_B)	M_{tot} (μ_B)
$\tilde{\rho}$	3.063	3.598	2.858	3.183
ρ_λ	3.283	4.000	3.289	3.999
$\rho_{\overline{\lambda}}$	3.267	4.000	3.274	4.000

used to obtain charge neutrality as described above. This is seen in table 3, where the total moments have the expected integer value 4 μ_B for the charge densities ρ_λ and $\rho_{\overline{\lambda}}$. As above for CrAs, it is not important whether the Green function is normalized by factors which vary along the integration contour or by factors which are chosen in an average way. The local moments inside the Mn cell exhibit the same trend as the total moments with an unphysical reduction of about 0.2 μ_B and 0.4 μ_B if the Fermi level is adjusted.

The difference in the magnetic moment is associated with a difference in the density of states, since the spin splitting of the density of states is essentially determined by the product of the magnetic moment with the almost constant exchange integral. The effect is clearly seen in figure 2, where the local density of states inside the Mn cell is plotted for energies in the vicinity of the Fermi level. Whereas the density of the states obtained by Green-function normalization is in good agreement with previous LDA calculations [34–37], the density of the states obtained by Fermi level adjustment is considerably different. The majority states are then shifted to higher energies by about 0.15 eV and the minority states to lower energies by about 0.35 eV so that the spin splitting is reduced by about 0.5 eV in line with the reduced moment. Figure 2 shows almost no difference between the densities of states calculated with the two different normalizations of the Green function. Thus for a good description of the Mn states in $Ga_{15}MnN_{16}$ it is important that the Fermi level is determined correctly, for instance by Lloyd's formula, and that the charge density is consistent with this Fermi level, whereas it is relatively unimportant how the normalization factors for the Green function are chosen.

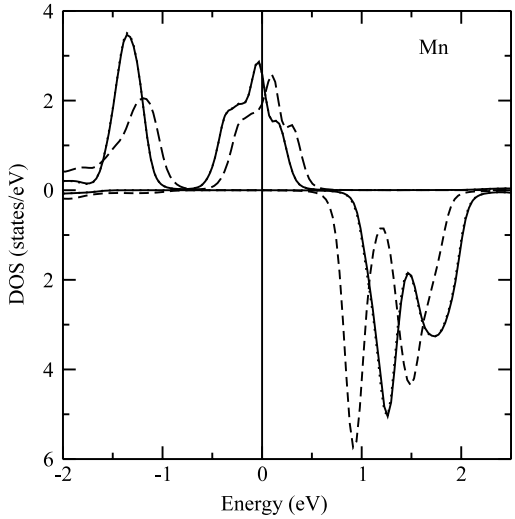

Figure 2. Calculated local density of states as a function of energy relative to E_F for the Mn atom in a $Ga_{15}MnN_{16}$ supercell. The dashed, solid and dotted lines were calculated for the charge densities $\tilde{\rho}$, ρ_λ and $\rho_{\overline{\lambda}}$ defined in the text. The majority (minority) spin results are shown in the upper (lower) part of the figure. Note that the dotted and solid lines nearly fall on top of each other so that the dotted lines are hardly visible.

5.3. $Si_{12}Fe_8$

In metal–semiconductor junctions the adjustment of the Fermi level to obtain charge neutrality leads to large errors for the energetic positions of the semiconducting states in the junction. Away from the interface the metallic and semiconducting regions of the junction should approach their bulk like behaviour. This means that in the inner layers of the semiconducting region the Fermi level should be positioned in the gap which cannot be obtained if the Fermi level is adjusted to obtain charge neutrality. For instance, a calculation with $l_{max} = 3$ puts the Fermi level into the upper part of the valence band of Si and consequently raises the semiconducting states in the junction compared to the metallic states. This unphysical band bending effect is particularly troubling for systems with many layers for which the tight-binding (TB) version of the KKR Green-function method would be an ideal tool since its computing effort scales only linearly with the number of layers [38].

The questions of how the band bending can be avoided and how the TB-KKR method can be applied for systems with many semiconducting layers were the main motivation for the present work. The example considered here was a periodically repeated system consisting of twelve Si layers and four Fe layers stacked in the 100-direction. A perfect matching was assumed between the bcc structure of Fe with lattice parameter $a = 0.2754$ nm chosen as in [39] and the diamond structure of Si with $a = 0.5508$ nm chosen twice as large. Geometrically, the system is rather simple since the diamond lattice can be obtained from the bcc lattice by omitting every second atom. Each Fe layer contained two Fe atoms and each Si layer one Si atom and one empty sphere, which was used to improve the angular momentum convergence. As above for $Ga_{1-x}Mn_xN$ any relaxation of the atoms in the interface region was neglected.

Figure 3 shows the calculated local densities of states inside the cells of the Fe and Si atoms with largest distance from the interface. The behaviour of the Fe and Si states is quite different. Whereas the different ways to obtain charge neutrality lead to barely visible changes for the Fe states, the Si states are clearly affected. Fermi level adjustment leads to Si states which are about 0.3 eV higher in energy than the Si states calculated with normalization factors which vary along the integration contour. For the charge density obtained with a constant normalization factor the shift of the Si states to higher energies is partly reduced, but still amounts to about 0.1 eV.

Under the assumption that the main reason for the shift of the states can be attributed to a change of the average potential in the atomic unit cell, the energy of the core levels is a useful

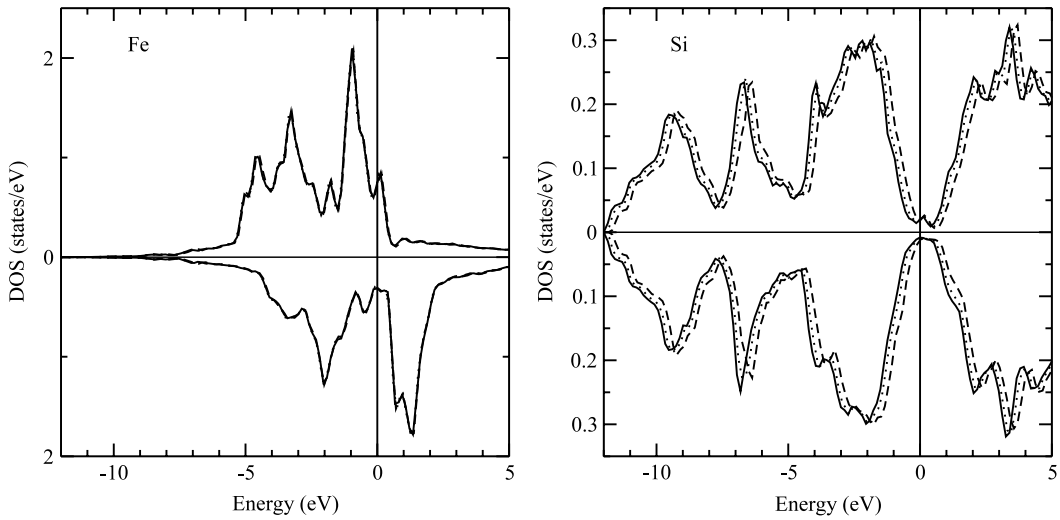

Figure 3. Calculated local density of states for the Fe and Si atoms with largest distance from the interface in a periodic $Si_{12}Fe_8$ multilayer as a function of energy relative to E_F. The dashed, solid and dotted lines were calculated for the charge densities $\tilde{\rho}$, ρ_λ and $\rho_{\overline{\lambda}}$ defined in the text. The majority (minority) spin results are shown in the upper (lower) part of the figure. Note that different scales are used for the left and right picture and that for Fe the different lines nearly fall on top of each other.

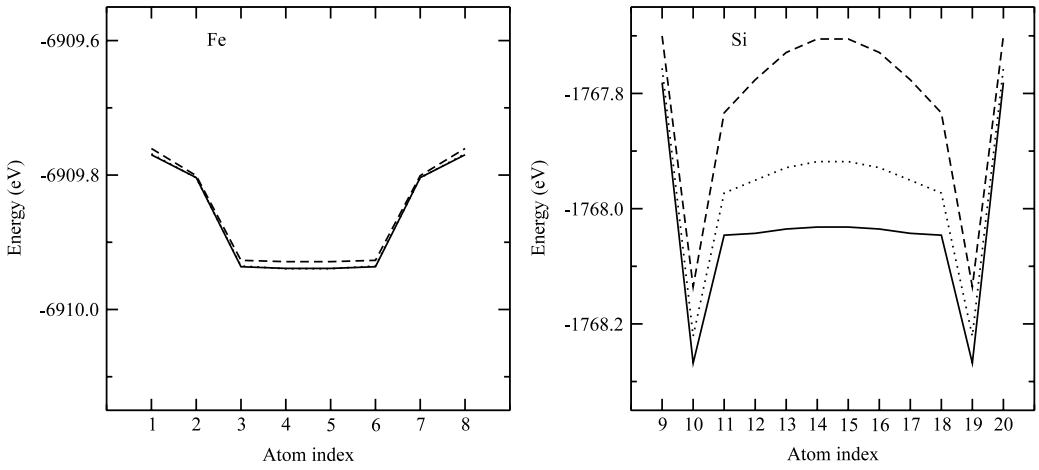

Figure 4. Calculated 1s core level energies relative to the Fermi level in a $Si_{12}Fe_8$ periodic multilayer. The dashed, solid and dotted lines were calculated for the charge densities $\tilde{\rho}$, ρ_λ and $\rho_{\overline{\lambda}}$ defined in the text.

measure for analysing the effect of the normalization of the Green function in the different layers of the multilayer, since the core states respond to the average potential in a similar way as the valence and conduction states. The energies of the 1s states are plotted in figure 4, which shows that away from the interface the energy of Si 1s states is almost constant if the Green function is normalized along the integration contour with factors determined by Lloyd's formula, whereas Fermi level adjustment clearly produces a band bending with an upward shift of about 0.3 eV in the middle of the semiconducting region in agreement with the DOS in figure 3. The size of the unphysical band bending is reduced to a maximum of about 0.1 eV in the middle of the semiconducting region, if the Green function is simply multiplied by a constant factor determined from the total charges calculated with and without Lloyd's formula. This shows that such a simple multiplication, which worked well to obtain integer moments for half-metallic CrAs and in $Ga_{1-x}Mn_xN$, is not sufficient to obtain a correct alignment of the states in metal–semiconductor junctions. For that purpose a Green-function normalization for each energy on the integration contour with factors determined by Lloyd's formula was found to be necessary.

6. Conclusion

A normalization procedure for the KKR Green-function method was developed which is able to compensate the charge density error which arises from the angular momentum truncation of the multiple-scattering representation of the Green function. The procedure is based on the use of Lloyd's formula to determine the Fermi level and to calculate normalization factors, which can be used to normalize the KKR Green function along complex energy integration contours. It was shown how the difficulty arising from the divergence

of the real part of the Green function can be circumvented and that the normalization procedure improves the charge density so that integer moments for a half-metallic system and correct band alignments in metal–semiconductor junctions can be calculated. It is expected that the improved charge density will be particularly useful for dilute magnetic semiconductors treated by the KKR coherent potential approximation (KKR-CPA) and for thick metal–semiconductor junctions treated by the TB-KKR Green-function method since in these systems a correct normalization is indispensable for avoiding large errors in the electronic states.

Acknowledgments

It is my pleasure to thank Professor P H Dederichs for his continued interest in this work and for careful reading of the manuscript.

Appendix A. $\Delta\alpha$ and Δt matrices

These matrices are defined as

$$\Delta\alpha^n_{LL'}(E) = \delta_{LL'} + \int_n \mathrm{d}\mathbf{r}\, S^{r,n}_L(\mathbf{r};E)[V^n(\mathbf{r}) - V^{r,n}(\mathbf{r})] \times R^n_{L'}(\mathbf{r};E) \tag{A.1}$$

and

$$\Delta t^n_{LL'}(E) = \int_n \mathrm{d}\mathbf{r}\, R^{r,n}_L(\mathbf{r};E)[V^n(\mathbf{r}) - V^{r,n}(\mathbf{r})] \times R^n_{L'}(\mathbf{r};E). \tag{A.2}$$

For the special choice of free space as reference system these definitions agree with the usual expressions

$$\alpha^n_{LL'}(E) = \delta_{LL'} + \int_n \mathrm{d}\mathbf{r}\, H_L(\mathbf{r};E)V^n(\mathbf{r})R^n_{L'}(\mathbf{r};E) \tag{A.3}$$

and

$$t^n_{LL'}(E) = \int_n \mathrm{d}\mathbf{r}\, J_L(\mathbf{r};E)V^n(\mathbf{r})R^n_{L'}(\mathbf{r};E). \tag{A.4}$$

In the equations above $S^{r,n}_L$ and $R^{r,n}_L$ are regular and irregular single-scattering solutions of the reference system and R^n_L regular single-scattering solutions of the system. They are defined by integral equations

$$S^{r,n}_L(\mathbf{r};E) = \sum_{L'} \beta^{r,n}_{LL'}(E)H_{L'}(\mathbf{r},E) + \int_n \mathrm{d}\mathbf{r}' S^{r,n}_L(\mathbf{r}';E)V^n(\mathbf{r}')G^0(\mathbf{r}',\mathbf{r};E) \tag{A.5}$$

$$R^{r,n}_L(\mathbf{r};E) = J_L(\mathbf{r};E) + \int_n \mathrm{d}\mathbf{r}' R^{r,n}_L(\mathbf{r}';E)V^{r,n}(\mathbf{r}')G^0(\mathbf{r}',\mathbf{r};E) \tag{A.6}$$

$$R^n_{L'}(\mathbf{r};E) = J_{L'}(\mathbf{r};E) + \int_n \mathrm{d}\mathbf{r}' G^0(\mathbf{r},\mathbf{r}';E)V^n(\mathbf{r}')R^n_{L'}(\mathbf{r};E), \tag{A.7}$$

where the matrix $\beta^{r,n}$ is defined as

$$\beta^{r,n}_{LL'}(E) = \delta_{LL'} - \int_n \mathrm{d}\mathbf{r}\, S^{r,n}_L(\mathbf{r};E)V^{r,n}(\mathbf{r})J_{L'}(\mathbf{r};E). \tag{A.8}$$

Note that in (A.6) the symmetry $G^0(\mathbf{r}',\mathbf{r};E) = G^0(\mathbf{r},\mathbf{r}';E)$ was used and that (A.6) is given in a form which is useful below.

For the calculations it is convenient that the changes $\Delta\alpha$ and Δt can be expressed in terms of α and t matrices of system and reference systems without the need to evaluate the additional integrals in (A.1) and (A.2). These expressions are

$$\Delta t^n_{LL'}(E) = t^n_{LL'}(E) - t^{r,n}_{LL'}(E) \tag{A.9}$$

and

$$\sum_{L''} \alpha^{r,n}_{LL''}(E)\Delta\alpha^n_{L''L'}(E) = \alpha^n_{LL'}(E), \tag{A.10}$$

which by taking determinants and logarithms leads to the result

$$\ln\det|\Delta\alpha^n_{LL'}(E)| = \ln\det|\alpha^n_{LL'}(E)| - \ln\det|\alpha^{r,n}_{LL'}(E)| \tag{A.11}$$

which was used for the evaluation of Lloyd's formula (9). The equivalence of (A.9) with (A.2) can be shown, if the function $R^{r,n}_L$, which multiplies V^n in (A.2), is replaced by the right-hand side of (A.6) and if the function $R^n_{L'}$, which multiplies $V^{r,n}$, is replaced by the right-hand side of (A.7). This leads to

$$\begin{aligned}\Delta t^n_{LL'}(E) = {} & \int_n \mathrm{d}\mathbf{r}\, J_L(\mathbf{r};E)V^n(\mathbf{r})R^n_{L'}(\mathbf{r};E) \\ & + \int_n \mathrm{d}\mathbf{r} \int_n \mathrm{d}\mathbf{r}' R^{r,n}_L(\mathbf{r}';E)V^{r,n}(\mathbf{r}')G^0(\mathbf{r}',\mathbf{r};E) \\ & \times V^n(\mathbf{r})R^n_{L'}(\mathbf{r};E) \\ & - \int_n \mathrm{d}\mathbf{r}\, R^{r,n}_L(\mathbf{r};E)V^{r,n}(\mathbf{r})J_{L'}(\mathbf{r};E) \\ & - \int_n \mathrm{d}\mathbf{r} \int_n \mathrm{d}\mathbf{r}' R^{r,n}_L(\mathbf{r};E)V^{r,n}(\mathbf{r})G^0(\mathbf{r},\mathbf{r}';E) \\ & \times V^n(\mathbf{r}')R^n_{L'}(\mathbf{r}';E).\end{aligned} \tag{A.12}$$

Here second and fourth terms cancel, the first term agrees with (A.4) and the third term agrees with $t^{r,n}_{L'L}(E)$ and thus, because t matrices are symmetric matrices, with $t^{r,n}_{LL'}(E)$. Similarly to (A.12), again by cancellation of terms with double integrals, the result

$$\begin{aligned}\Delta\alpha^n_{LL'}(E) = {} & \delta_{LL'} + \sum_{L''} \beta^{r,n}_{LL''}(E) \\ & \times \int_n \mathrm{d}\mathbf{r}\, H_{L''}(\mathbf{r};E)V^n(\mathbf{r})R^n_{L'}(\mathbf{r};E) \\ & - \int_n \mathrm{d}\mathbf{r}\, S^{r,n}_L(\mathbf{r};E)V^{r,n}(\mathbf{r})J_{L'}(\mathbf{r};E)\end{aligned} \tag{A.13}$$

is obtained from (A.1) by use of (A.5) and (A.7). Here the first integral agrees with $\alpha^n_{L''L'}(E) - \delta_{L''L'}$ and the second integral with $\delta_{LL'} - \beta^{r,n}_{LL'}(E)$. Thus, in matrix notation, (A.13) can written as $\Delta\alpha = 1 + \beta^r(\alpha - 1) - (1 - \beta^r)$, which simplifies to $\Delta\alpha = \beta^r\alpha$. This result is equivalent to (A.10), since β matrices are inverses of α matrices as has been shown in [11].

Appendix B. Free space correction term

A straightforward way to avoid the infinite sum in (17) seems to remove the Hankel functions in terms of Bessel functions by

$$\mathrm{Im}\left[\mathrm{i}h_l^{(1)}(r\sqrt{E})\,j_l(r\sqrt{E})\right] = \begin{cases} j_l^2(r\sqrt{E}) & \text{for } E > 0 \\ 0 & \text{for } E < 0, \end{cases} \tag{B.1}$$

which is valid for real energy E, and to use

$$\sum_{-m}^{m} Y_{lm}(\hat{\mathbf{r}})Y_{lm}(\hat{\mathbf{r}}) = \frac{2l+1}{4\pi} \tag{B.2}$$

and

$$\sum_{l=0}^{\infty}(2l+1)\,j_l^2(r\sqrt{E}) = 1. \tag{B.3}$$

This leads to

$$\mathrm{Im}\left[\sum_{l>l_{\max}}^{\infty} J_L(\mathbf{r};E)H_L(\mathbf{r};E)\right] = -\frac{1}{\sqrt{E}}4\pi\left[1-\sum_{l=0}^{l_{\max}} j_l^2(r\sqrt{E})\right]. \tag{B.4}$$

Although the analytical continuation of the right-hand side of (B.4) into the complex energy plane is straightforward, it cannot be used for the calculation of normalization factors, since it significantly differs from the left-hand side of (B.4) and, moreover, since it was found to lead to normalization factors with unpleasant values far from one. Nevertheless, the left-hand side of (B.4) can easily be integrated over space and energy and its contribution to the total charge is rather small. For the systems studied its value was always less than 0.000 65 and 0.000 02 for $l_{\max} = 3$ and $l_{\max} = 4$. Thus the two-step procedure explained above (see (18) and (19)) seems to be well justified, in particular because of its rapid $l_{\max}$ convergence.

Appendix C. Cell integration of the charge density

Charge density integration over a cell is done by multiplying the integrand with a step function $\Theta^n(\mathbf{r})$, which is equal to 1 in the cell n and zero otherwise. This enables to extend the integration over all space

$$\int_n \mathrm{d}\mathbf{r}\,\tilde{\rho}(\mathbf{r}+\mathbf{R}^n) = \int \mathrm{d}\mathbf{r}\Theta^n(\mathbf{r})\tilde{\rho}(\mathbf{r}+\mathbf{R}^n). \tag{C.1}$$

By use of the spherical harmonic expansions

$$\Theta^n(\mathbf{r}) = \sum_L \Theta_L^n(r)Y_L(\mathbf{r}) \tag{C.2}$$

and

$$\tilde{\rho}(\mathbf{r}+\mathbf{R}^n) = \sum_L^{2l_{\max}} \tilde{\rho}_L^n(r)Y_L(\mathbf{r}) \tag{C.3}$$

the result

$$\int_n \mathrm{d}\mathbf{r}\,\tilde{\rho}(\mathbf{r}+\mathbf{R}^n) = \int_0^{\infty} \mathrm{d}r r^2 \sum_L^{2l_{\max}} \Theta_L^n(r)\tilde{\rho}_L^n(r) \tag{C.4}$$

follows. Here it is important to note that (C.3) only contains terms with $l \leqslant 2l_{\max}$, which by orthogonality of spherical harmonics leads to the finite sum in (C.4). The cut-off at $2l_{\max}$ in (C.3) is a natural consequence of $l_{\max}$ truncation for the Green function. This can be seen if the expansion $G^0(\mathbf{r},\mathbf{r}';E) = \sum_L Y_L(\mathbf{r})g_l(r,r';E)Y_L(\mathbf{r}')$ for the free space Green function, truncated to terms with $l \leqslant l_{\max}$, and $J_{L'}(\mathbf{r};E) = j_{l'}(r\sqrt{E})Y_{L'}(\mathbf{r})$ are used in (A.7). The right-hand side of (A.7) is then given as a finite combination of spherical harmonics $Y_L(\mathbf{r})$ multiplied with functions which depend on the radial variable r alone. This means that $R_{L'}^n(\mathbf{r};E)$ can be written as

$$R_{L'}^n(\mathbf{r};E) = \sum_L^{l_{\max}} Y_L(\mathbf{r})R_{LL'}^n(r;E) \tag{C.5}$$

and that the Green function (4) can represented as a finite double sum over products of spherical harmonics. Consequently, the charge density can be represented as

$$\tilde{\rho}(\mathbf{r}+\mathbf{R}^n) = \sum_{L'}^{l_{\max}}\sum_{L''}^{l_{\max}} Y_{L'}(\mathbf{r})\tilde{\rho}_{L'L''}^n(r)Y_{L''}(\mathbf{r}), \tag{C.6}$$

from which the expansion coefficients $\tilde{\rho}_L^n(r)$ for use in (C.3) are found by multiplication with $Y_L(\mathbf{r})$ and integration over the angles. Since angular integrals over the three spherical harmonics vanish for $l > l' + l''$, coefficients $\tilde{\rho}_L^n(r)$ with $l > 2l_{\max}$ do not appear in (C.3). This means that apart from the angular momentum truncation of the Green function no further approximation is necessary for the charge density integrals.

Appendix D. Complex energy contour

The contour starts on the negative real energy axis at energy E_A, which is chosen below the valence and above the core states. From E_A the contour goes to $E_B = E_A + 2Ni\pi kT$, where N is a chosen integer, on a line parallel to the imaginary axis and from E_B to infinity on a line parallel to the real axis. Compared to the integral along the real axis from E_A to infinity, the integral along the contour omits the residues at the first N Matsubara energies $E_n = E_\mathrm{F} + (2n-1)i\pi kT$ with $n = 1, 2, \ldots, N$, which must be added to the contour integral separately. The contour from E_B to infinity is divided into a part from E_B to $E_C = E_\mathrm{F} - 30kT + 2Ni\pi kT$ and a part from E_C to infinity. For the integration from E_C to infinity a special four-point Gauss rule for the Fermi–Dirac weight function was developed according to the description given in [40]. Standard Gauss–Legendre rules were used between E_A and E_B with five points and between E_B and E_C with 16 points except for $Ga_{1-x}Mn_xN$, where 24 points were necessary for accurate integration over the Ga 3d states. Note that the Fermi–Dirac function can be neglected between E_B and E_C, where it differs from one by less than 10^{-13}. With the choice $N = 15$ the total number of mesh points was 48 for $Ga_{1-x}Mn_xN$ and 40 for the other systems.

References

[1] Treusch J and Sandrock R 1966 *Phys. Status Solidi* **16** 487
[2] Kaprzyk S and Bansil A 1990 *Phys. Rev.* B **42** 7358
[3] Zhang X-G and Butler W H 1992 *Phys. Rev.* B **46** 7433
[4] Tatarchenko A F and Kulikov N 1994 *Phys. Rev.* B **50** 8266
[5] Kaprzyk S 1997 *Acta Phys. Pol.* A **91** 135
[6] Moghadam N Y, Stocks G M, Zhang X-G, Nicholson D M C, Shelton W A, Wang Y and Faulkner J S 2001 *J. Phys.: Condens. Matter* **13** 3073

[7] Zeller R 2005 *J. Phys.: Condens. Matter* **17** 5367
[8] Ham F S and Segall B 1961 *Phys. Rev.* **124** 1786
[9] Zeller R, Deutz J and Dederichs P H 1982 *Solid State Commun.* **44** 993
[10] Wildberger K, Lang P, Zeller R and Dederichs P H 1995 *Phys. Rev.* B **52** 11502
[11] Zeller R 2004 *J. Phys.: Condens. Matter* **16** 6453
[12] Drittler B, Weinert M, Zeller R and Dederichs P H 1989 *Phys. Rev.* B **39** 930
[13] Ebert H and Zeller R The SPR-TB-KKR package http://olymp.cup.uni-muenchen.de/ak/ebert/SPR-TB-KKR/
[14] Andersen O K, Postnikov A V and Savrasov S Yu 1992 *Application of Multiple Scattering Theory to Materials Science* (*MRS Symposia Proceedings* No. 253) ed W H Butler, P H Dederichs, A Gonis and R L Weaver (Pittsburgh, PA: Materials Research Society) p 37
[15] Andersen O K, Jepsen O and Krier G 1994 *Lectures on Methods of Electronic Structure Calculations* ed V Kumar, O K Andersen and A Mookerjee (Singapore: World Scientific)
[16] Szunyogh L, Újfalussy B, Weinberger P and Kollar J 1994 *Phys. Rev.* B **49** 2721
[17] Zeller R, Dederichs P H, Újfalussy B, Szunyogh L and Weinberger P 1995 *Phys. Rev.* B **52** 8807
[18] Papanikolaou N, Zeller R and Dederichs P H 2002 *J. Phys.: Condens. Matter* **14** 2799
[19] Andersen O K and Woolley R G 1973 *Mol. Phys.* **26** 905
[20] Stefanou N, Akai H and Zeller R 1990 *Comput. Phys. Commun.* **60** 231
[21] Stefanou N and Zeller R 1991 *J. Phys.: Condens. Matter* **3** 7599
[22] Drittler B, Weinert M, Zeller R and Dederichs P H 1991 *Solid State Commun.* **79** 31
[23] Ghosh S, Biava D A, Shelton W A and Johnson D D 2006 *Phys. Rev.* B **73** 085106
[24] Vosko S H, Wilk L and Nusair M 1980 *Can. J. Phys.* **58** 1200
[25] Akinaga H, Manago T and Shirai M 2000 *Japan. J. Appl. Phys.* **39** L1118
[26] Galanakis I and Mavropoulos P 2003 *Phys. Rev.* B **67** 104417
[27] Galanakis I, Dederichs P H and Papanikolaou N 2002 *Phys. Rev.* B **66** 134428
[28] Sasioglu E, Galanakis I, Sandratskii L M and Bruno P 2005 *J. Phys.: Condens. Matter* **17** 3915
[29] Korhonen T, Settels A, Papanikolaou N, Zeller R and Dederichs P H 2000 *Phys. Rev.* B **62** 452
[30] Birch J 1978 *J. Geophys. Res.* **83** 1257
[31] Asato M, Settels A, Hoshino T, Asada T, Blügel S, Zeller R and Dederichs P H 1999 *Phys. Rev.* B **60** 5202
[32] de Paiva R, Nogueira R A and Alves J L A 2006 *J. Phys.: Condens. Matter* **18** 8589
[33] Kronik L, Jain M and Chelikowsky J R 2002 *Phys. Rev.* B **66** 041203
[34] Sato K and Katayama-Yoshida H 2001 *Japan. J. Appl. Phys.* **40** L485
[35] Sanyal B, Bengone O and Mirbt S 2003 *Phys. Rev.* B **68** 205210
[36] Sandratskii L M, Bruno P and Kudrnovsky J 2004 *Phys. Rev.* B **69** 195203
[37] de Paiva R, Alves J L A, Nogueira R A, Leite J R and Scolfaro L M R 2004 *Braz. J. Phys.* **34** 647
[38] Wildberger K, Zeller R and Dederichs P H 1997 *Phys. Rev.* B **55** 10074
[39] Freyss M, Papanikolaou N, Bellini V, Zeller R and Dederichs P H 2002 *Phys. Rev.* B **66** 014445
[40] Sagar R P 1991 *Comput. Phys. Commun.* **66** 271